1   **Investigation of the functional relationship between antecedent rainfall and the probability**

2   **of debris flow occurrence in Jiangjia Gully, China**

3   Shaojie Zhang[1], Xiaohu Lei[1,4], Hongjuan Yang[1], Kaiheng Hu[1], Juan Ma[2], Dunlong Liu[3], Fanqiang Wei[4]

4   1. Key Laboratory of Mountain Hazards and Earth Surface Process, Institute of Mountain Hazards and Environment,

5   Chinese Academy of Sciences, Chengdu 610041, China

6   2. China Institute for Geo-Environment Monitoring, Beijing, 100081

7   3. College of Software Engineering, Chengdu University of Information and Technology, Chengdu, 610225, China

8   4. Chongqing Institute of Green and Intelligent Technology, Chinese Academy of Sciences, Chongqing 400714,

9   China

10   Correspondence to: Shaojie Zhang, E-mail: sj-zhang@imde.ac.cn; Kaiheng Hu, E-mail: khhu@imde.ac.cn

11   **Abstract**

12   A larger antecedent effective precipitation (AEP) indicates a higher probability of a debris flow

13   (P_{df}) being triggered by subsequent rainfall. Scientific topics surrounding this qualitative conclusion

14   that can be raised, including what kinds of variation rules do they follow, and whether there is a

15   boundary limit. To answer these questions, Jiangjia Gully in Dongchuan, Yunnan province, China,

16   is chosen as the study area, and a numerical calculation, rainfall scenario simulation, and Monte

17   Carlo integration method have been used to calculate the occurrence probability of debris flow under

18   different AEP conditions and derive the functional relationship between P_{df} and AEP. The

19   relationship between P_{df} and AEP can be quantified by a piecewise function. P_{df} is equal to 15.88%

20   even AEP reaches 85 mm indicating that debris flow in nature has an extremely small probability

21   compared to the rainfall frequency. Data from 1094 rainfall events and 37 historical debris flow

22 events are collected to verify the reasonability of the functional relationship. The results indicate

23 that the piecewise function are highly correlated with the observation results. Our study confirms

24 the correctness of the qualitative description of the relationship between AEP and P_{df}, clarifies that

25 debris flow is a small probability event compared to rainfall frequency, and quantitatively reveals

26 the evolution law of debris flow occurrence probability with AEP, which can provide a clear

27 reference for the early warning of debris flows.

28 **Keywords:** Debris flow, antecedent effective rainfall, Dens-ID, Monte Carlo method

30 **1 Introductions**

31   The antecedent effective precipitation (AEP) likes a Trojan horse lurking inside a loose soil

32 mass, which can cooperate with subsequent rainfall at any time to trigger debris flow in a debris-

33 flow gully. The AEP is equivalent to the precipitation preserved in soil mass before the triggering

34 rainfall process; it represents the saturation degree of loose soil mass (Segoni et al., 2018a;

35 Leonarduzz and Molnar, 2020). Therefore, the soil moisture that has accumulated from antecedent

36 rainfall since the beginning of a rainfall season has a significant influence on how new storm rainfall

37 interacts with the loose soil mass within a gully (Fiorillo and Wilson, 2004; Long et al., 2020). The

38 increase in AEP can decrease the shear strength of a loose solid material provided by shallow

39 landslides or channel erosion (Papa, et al., 2013; Senthilkumar et al., 2017; Liu et al., 2020), as a

40 consequence, the supply rate of solid material resources can be significantly enhanced in the

41 subsequent rainfall process (Wei et al., 2008; Bennett et al., 2014; Zhang et al., 2020). Additionally,

42 increased AEP and moisture content have been shown to enhance rainfall-induced surface runoff in

43 a variety of environments (Tisdall, 1951; Luk, 1985; Le Bissonnais et al., 1995; Castillo et al., 2003;

44   Jones et al., 2017; Hirschberg et al., 2021). Thus, AEP plays an important role in the formation of

45   debris flows (Hong et al., 2018).

46   Rainfall thresholds represent the difficulty degree of debris flow triggered by rainfall (Marra

47   et al., 2017). Investigations including the influence of AEP on the rainfall threshold can be helpful

48   to examining the relationship between AEP and debris flow occurrence. Currently, the relationship

49   between the AEP and rainfall threshold indicates that there is a negative correlation between the

50   AEP and rainfall conditions that trigger debris flows (Huang, 2013). AEP also represents the

51   saturation degree of loose soil mass (Zhao et al., 2019a; Abraham et al., 2021), and integrating soil

52   moisture with rainfall thresholds has been proven effective in improving prediction performance

53   (Segoni et al., 2018a; Zhao et al., 2019b; Abraham et al., 2020). Scholars also have attempted to

54   analyze the influence of antecedent soil moisture on the rainfall threshold triggering debris flow

55   (Cui et al., 2007; Hu et al., 2015), and there is still a negative correlation between antecedent soil

56   moisture and triggering rainfall conditions (Chen et al., 2017) just like the relationship between AEP

57   and rainfall threshold. The above investigations show that increasing in AEP can significantly

58   decrease the rainfall conditions for triggering a debris flow, which in turn means that debris flow is

59   more likely to occur. Generally, the qualitative description of 'the greater the AEP, the higher the

60   probability (P_{df}) of subsequent rainfall triggering the debris flow (De Vita et al., 2000; Bel et al.,

61   2017)' has gradually become a consensus. Therefore, discovering a specific function to describe this

62   qualitative description is helpful to further demonstrating the above consensus, revealing a certain

63   evolutionary law of debris flow with rainfall in nature.

64   To quantify the evolution law of P_{df} with the changing AEP, a numerical model denoted as the

65   Dens-ID can correlate the rainfall parameters (I and D) with the debris flow density (Zhang et al.,

66   2020; Long et al., 2020; Zhang et al., 2023), and it has been used to construct the rainfall intensity-

67   duration (ID) threshold curves under different AEP conditions. The ID threshold curves with upper

68   and lower bounds can delineate the closed region in the ID coordinate system, which represents the

69   set of all rainfall conditions that can trigger debris flow at a certain AEP. Consequently, the

70   probability of natural rainfall falling into a closed region is equivalent to P_{df}, which can then be

71   calculated based on Monte Carlo integration. The next section introduces the basic information of

72   study area including the rainfall and debris flow event data collected from the study area. The third

73   section addresses how to establish the functional relationship between the AEP and Pdf using the

74   Dens-ID and Monte Carlo integration method. Section 4, 5 and 6 discuss the results and state the

75   conclusions of this study, respectively.

76 **2 Study areas**

77   The Jiangjia Gully (JJG) is a primary tributary of the Xiaojiang River, which is located in the

78   Dongchuan District of Kunming City, Yunnan Province, China (Fig.1). As shown in Fig.1, JJG has

79   a drainage area of 48.6 km^2 with elevations ranging from 1040to 3260 m. In this gully, the relative

80   relief from the ridge to the valley reaches 500 m, and most of the slope gradient is greater than 25°.

81   Slopes within JJG are covered by abundant loose soil with a thickness of more than ten meters.

82   Shallow landslides are frequently triggered by intense rainfall processes in JJG, providing a large

83   number of solid materials for debris flow (Yang et al., 2022). Before 1979, the Menqian and

84   Duozhao gullies are the two main tributaries of JJG, accounting for 64.7% of the entire drainage

85   area. The upstream areas of the two main tributaries are the initiation zones of the debris flows, and

86   the channels of the upstream tributaries are narrow and V-shaped (Zhang et al., 2020). However,

87   several check dams have been constructed in the Duozhao gully since 1979, which have

88   significantly reduced debris flow activity in this sub-gully (Zeng et al., 2009). Currently, Menqian

89   Gully with the area of 13.2 km^2 is the primary source area. The slope gradient of its both sides is

90   very steep, e.g., the mean slope in Menqian Gully is 32° and the maximum slope can reach 70°.

Bedrock that mainly consists of slates formed in lower Proterozoic crops out in the unvegetated or sparsely vegetated lower part. The bedrock is fragmented and mostly disintegrates into clasts with the size more than 20 mm. The upper part of the bedrock is lain by soil mantles with thicknesses of 0.5–20 m, which are covered by grasses and shrubs, or are used for terrace farming. The soil mantle is poorly sorted and composed of particles from clay to boulder. The translational zone from the upper to the lower parts of the slope is prone to shallow landslides. Some landslides directly evolve into debris flows, while the others release sediment to the channel, which is mobilized by runoff in debris flow events (Yang et al., 2022).
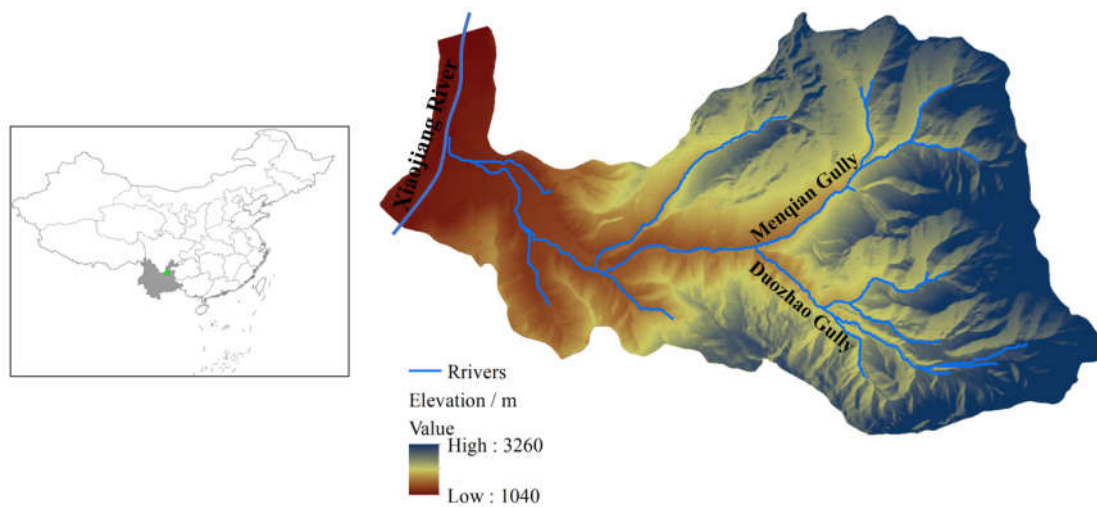
Fig.1 Location of JJG

Steep terrain provides a beneficial potential energy condition for transporting a large amount of loose solid materials from JJG to Xiaojiang River. Consequently, debris flows in JJG can be easily triggered by high-intensity rainstorm or long-duration rainfall processes (Zhang et al., 2020). The solid material necessary for a debris flow in a gully may be from shallow landslides (Iverson et al., 1997; Gabet and Mudd, 2006; Zhang et al., 2020; Long et al., 2020) or runoff-induced bed erosions (Berti and Simoni, 2005; Coe et al., 2008; Tang et al., 2020; Bernard and Gregoretti, 2021). In JJG, shallow landslides are the main sources for the solid material supply (Zhang et al., 2014; Liu et al., 2016; Yang et al., 2022), which is consistent with the assumptions of Dens-ID (Zhang et al., 2020). Thus, JJG is used as the study zone for deriving the function that describes the relationship between

110   AEP and P_{df}.

3 Methods and data

3.1 Dens-ID

Debris flow gullies characterized by a solid source supply from landslides are widely distributed in southwest China (Zhang et al., 2014). For this type of debris flow gully, our previous study proposed Dens-ID aiming at correlating debris-flow density to rainfall parameters based on water-soil coupling mechanism (Zhang et al., 2020; Long et al., 2020). Den-ID assumes debris flow to be a water-soil mixture, it contains three core simulating contents including hydrological simulation, water-soil coupling to calculate the water-soil-mixture density, and correlating density to rainfall parameters.

(1) Simulating hydrological process: the purpose is to provide parameters for estimating rainfall-induced runoff and the supply volume of rainfall-induced loose solid materials. Based on the digital elevation model (DEM) of a gully, Den-ID can simulate the rainfall-induced runoff and water diffusion in the vertical direction within the soil mass. The rainfall infiltration border is controlled by Eq.1.

$$-D(\theta)\frac{\partial \theta}{\partial z} + K(\theta) = I(t) \qquad (1)$$

where θ is the soil water content; $D(\theta) = K(\theta)/(d\theta/d\psi)$, which represents the soil water diffusivity; z is the soil depth, which is positive downwards along the soil depth as the topsoil is taken as the origin point; $K(\theta)$ is the hydraulic conductivity; $I(t)$ is the rainfall intensity; and ψ is the soil matrix suction. When the rainfall intensity is less than the surface infiltration capacity, Eq. 1 is used to represent this physical process; whereas the case of precipitation intensity exceeding the infiltration capacity of topsoil means that the surface is saturated, and the excess precipitation

132   from the topsoil is converted into runoff. Therefore, the pressure infiltration of each grid cell is not

133   considered.

$$\frac{\partial \theta}{\partial t} = \frac{\partial}{\partial z}[D(\theta)\frac{\partial \theta}{\partial z}] - \frac{\partial K(\theta)}{\partial z} \qquad (2)$$

134

135   Eq. 2 is the Richard differential infiltration equation (Richards, 1931), which is used to describe the

136   water movement along the vertical direction within soil mass after precipitation infiltrates into

137   topsoil. Dens-ID uses the finite-difference method to solve Eqs. 1 and 2 and can provide the runoff

138   depth (denoted as $dw(i,t)$), soil water content, and soil matrix suction for each grid cell. Dens-ID

139   then calculates the runoff volume using runoff depth $dw(i, t)$ in Eq. 3.

$$V_w(t) = \sum_{t=1}^{T}\sum_{i=1}^{n} S_g * dw(i,t) \qquad (3)$$

140

141   where n represents the total number of grid cells that can generate runoff at time t, $V_w(t)$ represents

142   the total volume of runoff within a gully at time t, S_g represents the area of the grid cell generating

143   runoff, and T represents the total duration of a rainfall process.

144   (2) Calculating supply amount of loose solid materials and density of the water-soil mixture:

145   taking hydrological parameters such as soil water content and soil matrix suction as inputs, Dens-

146   ID uses Eqs. 4 and 5 to estimate the supply amount of rainfall-induced loose solid materials within

147   a gully. Eq. 4 calculates safety factor F_s of each grid cell as a function of the matrix suction and soil

148   moisture. $F_s > 1$ indicates that the grid cell is stable and cannot supply solid material to the gully,

149   whereas a grid with $F_s < 1$ can provide solid material in the form of a shallow landslide.

$$F_s = \frac{tan\,\varphi}{tan\,\beta} + \frac{c + \psi\,tan(\varphi^b)}{\gamma_t d_s \cos\beta \sin\beta} \qquad (4)$$

150

151   where F_s represents the safety factor of each grid cell, c is the soil cohesion force, φ is the internal

152   friction angle, φ^b is related to the matrix suction and is approximately equal to φ as the low matrix

153   suction is small, d_s is the soil depth, and ψ is the matrix suction which is a function of soil water

154   content and can be described by the Van Genuchten model (Van Genuchten, 1980).

155   Using d_s derived from Eq. 3 as input, Eq. 4 is used to estimate the total volume of solid

156   materials from all the instable grid cells during a rainfall process.

157    $$V_s(t) = \sum_{t=1}^{T} \sum_{j=1}^{m} S_g * ds(j,t)$$ (5)

158   where m represents the number of grid cells that can provide solid material at time t and $V_s(t)$ is the

159   total volume of solid material within a gully at time t. At time t, the density of the water-soil mixture

160   after full coupling between runoff and solid material can be calculated using Eq. 6.

161    $$\rho_{mix}(t) = \frac{\rho_w V_w(t) + \rho_s V_s(t)}{V_{mix}(t)}$$ (6)

162   where $\rho_{mix}(t)$ is the density of the water-soil mixture, ρ_w is the water density, ρ_s is the density of

163   the soil particles, and $V_{mix}(t)$ is the volume of the water-soil mixture, which is the sum of $V_w(t)$

164   and $V_s(t)$. $V_w(t)$ and $V_s(t)$ are the key variables that can be derived using Eqs. 3 and 5.

165   (3) Correlating density to rainfall parameters including rainfall intensity and duration: Dens-

166   ID firstly presets the density of the water-soil mixture as ρ_{mix}, it needs to simulate many rainfall

167   scenarios including long durations with low-intensity rainfall and short durations with high-intensity

168   rainfall in order to obtain a sufficient number of [D_i, l_i]. Using each [D_i, I_i] as input, Dens-ID then

169   can calculate the density using Eq.6. If the calculated density is equal to ρ_{mix}, the [D_i, I_i] combination

170   is saved by Dens-ID. After Dens-ID completes the trial calculations, all combination data of [D_i, I_i]

171   that satisfy the constraints of the preset density (ρ_{mix}) can be collected as a dataset. Each collected

172   [D_i, I_i] within the dataset corresponds to the preset ρ_{mix}, accordingly, Dens-ID can correlate rainfall

173   parameters (D and I) to debris flow density (Long et al., 2020). Dens-ID can derive ID threshold

174   curves by fitting the selected [D_i, I_i] data, and each ID curve corresponds to a debris flow density

175   value (Zhang et al., 2020). As the density of debris flow in JJG varies in a specific interval of 1.2–

176 2.3g/cm³ (Zhang et al., 2014; Zhuang et al., 2015; Long et al., 2020), the threshold curve that

177 corresponds to the boundary value can form a closed area with the I- and D-axes in the ID coordinate

178 system. The case of monitoring or forecasting rainfall falling into this closed area indicates that the

179 rainfall condition may trigger debris flow. The verification results in JJG show that Dens-ID can

180 effectively describe the mechanism and process of debris flow formation, and its prediction accuracy

181 is approximately 80.5%, which is 27.7% higher than that of statistical models (Zhang et al., 2020).

182 Such a high prediction accuracy can further indicate that the closed area formed by the derived ID

183 curves has a very reasonable location and coverage in the ID coordinate system, providing extremely

184 reliable analytical data in this study.

185 **3.2 JJG data for model Dens-ID**

186 The JJG datasets for Dens-ID are terrain data, hydrological parameters, and soil mechanical

187 parameters. The DEM is the basal data for deriving other terrain data, including slope length,

188 gradient, and river channels; the spatial resolution of the DEM is 0.5 m, and a DEM with a grid size

189 of 10 m was generated using the resampling technology in ArcGIS. The hydrological parameters

190 are related to the soil types within JJG; the five key parameters are the saturated soil water content,

191 residual soil water content, the two parameters of soil water characteristic curve including n and m,

192 and the infiltration rate of topsoil. The soil mechanical parameters are the soil cohesion force and

193 internal friction angle obtained through direct shear tests on the soil samples. Detailed data are

194 available in Zhang et al. (2020) and Long et al. (2020).

195 **3.3 Historical rainfall and debris flow data**

196   Rainfall data for the rainy seasons between 2006 and 2020 have been collected from the JJG

197   observation station, and it is necessary to identify each rainfall process from the long-term rainfall

198   sequences. Inter-event time (IET) is defined as the minimum time interval between two consecutive

199   rainfall pulses (Adams et al., 1986). IET has a strong influence on the rainfall event starting and

200   ending times (Bel et al., 2017), and Peres et al. (2018) has identified that IET depends on whether

201   the mean daily potential evapotranspiration (MDPE) is larger than precipitation within the IET. The

202   long observation of evaporation within JJG showed that MDPE is about 4 mm; precipitation during

203   IET >0.5 mm is considered the end of a rainfall process. Under this standard, 1094 rainfall events

204   and 37 debris flow events have been identified during the sampling period. Detailed rainfall data

205   information can be found in "appendix 1-1094 rainfall and 37 debris flow data.xlsx". The AEP listed

206   in this appendix is considered the weighted sum of the rainfall periods before the occurrence of

207   debris flow (Long et al., 2020) and it can be calculated using Eq. 7.

208    $$AEP = \sum_{i=1}^{n} K^n R_i \tag{7}$$

209   where AEP is the antecedent effective rainfall; K is the attenuation coefficient, which is equal to

210   0.78 based on the field test in JJG (Zhang et al., 2020); and n is the number of days preceding the

211   debris flow occurrence.

212   Based on the observed rainfall data, the 1094 AEPs are calculated using Eq. 7 and listed in

213   Appendix 1. The AEP corresponding to each rainfall event varies from 0–88 mm. Taking this

214   variation range as a reference, the variation range of the AEP input in the Dens-ID model is set

215   between 10 and 85 mm.. Dens-ID presets several AEP values including 10, 15, 20, 25, 30, 35, 40,

216   45, 50, 55, 60, 65, 70, 75, 80, 85. P_{df} can be calculated under different AEP conditions.

217   **3.4 Monte Carlo method for calculating the definite integral**

218   Because of the boundary of the debris-flow density in JJG (1.2–2.3g/cm^3), Dens-ID produces

219   the corresponding upper and lower boundary curves under a specific AEP condition. The two

220   boundary curves can be described using the power function.

221

$$\begin{cases} f(D)_{up} = I_{up} = \alpha_1 D^{\beta_1} & D\epsilon[a_1, b_1] \\ f(D)_{low} = I_{low} = \alpha_2 D^{\beta_2} & D\epsilon[a_2, b_2] \end{cases} \tag{8}$$

222   These two threshold curves can delineate an enclosed area in the ID coordinate system, denoted

223   as W_{ID}. The independent variable (D) and dependent variable (I) in Eq. 8 also form a closed

224   rectangular region in the ID coordinate system, denoted as R_{ID}. In the ID coordinate system, the

225   coverage of R_{ID} is larger than that of W_{ID}, as will be shown in detail in Section 4.1. Limited within

226   R_{ID}, any rainfall processes located in W_{ID} can trigger debris flow. If the probability of rainfall

227   process falling into the range of W_{ID} under random conditions is determined, the occurrence

228   probability of debris flow can be estimated. Many physical phenomena are stochastic in nature and

229   governed by stochastic partial differential equations with nondeterministic initial/boundary

230   conditions or integral equations (Peres and Cancelliere, 2014; Yan and Hong, 2014). Albert (1956)

231   proposed the Monte Carlo method for solving integral equations. This method is subsequently used

232   to estimate the peak flow and volume of debris flow (Donovan and Santi, 2017; Paola et al., 2017),

233   entrainment of the underlying bed sediment (Han et al., 2015), and risk assessment (Calvo and Savi,

234   2009; Li et al., 2021). The rainfall process is randomly selected within the R_{ID}, and the probability

235   of the chosen one falling into the W_{ID} can be determined using W_{ID}/R_{ID}. The physical meaning of

236   the Monte Carlo solving definite integral lies on calculating the area enclosed by the function curve

237   and horizontal axis. Therefore, the area of W_{ID} can be calculated by the difference in the definite

238   integral formula of the two equations in Eq. 7.

239

$$W_{ID} = S_{up} - S_{low} = \int_{a1}^{b1} f(D)_{up} dD - \int_{a2}^{b2} f(D)_{low} dD \tag{9}$$

where S_{up} and S_{low} represent the area enclosed by the two threshold curves and the horizontal axis, respectively, and a_1, b_1, a_2, and b_2 are the boundary values of D in the two curves. For the upper boundary line (or lower boundary), if the probability distribution function of D between [a1, b1] is p(D), Eq. 9 can be derived by substituting p(D) into Eq. 8.

$$\begin{cases} S_{up} = \int_{a_1}^{b_1} f(D)_{up} dD = \int_{a_1}^{b_1} \frac{f(D)_{up}}{p(D)} p(D) dD \approx \frac{1}{n} \sum_{k=1}^{n} \frac{f(D_i)_{up}}{p(D_i)} \\ S_{low} = \int_{a_2}^{b_2} f(D)_{low} dD = \int_{a_2}^{b_2} \frac{f(D)_{low}}{p(D)} p(D) dD \approx \frac{1}{n} \sum_{k=1}^{n} \frac{f(D_i)_{low}}{p(D_i)} \end{cases} \tag{10}$$

$$W_{ID} = \frac{1}{n} \sum_{k=1}^{n} \frac{f(D_i)_{up}}{p(D_i)} - \frac{1}{n} \sum_{k=1}^{n} \frac{f(D_i)_{low}}{p(D_i)} \tag{11}$$

where n represents the number of random samples drawn from the variation range of D, and $p(D_i)$ is the probability density distribution function of D in the interval [a_1,b_1] or [a_2,b_2]. The key to solving Eq. 10 depends on sampling from p(D). The following steps are used to explain how samples were taken using $p(D_i)$.

Step 1: Based on the probability density distribution function p(D), the cumulative probability distribution function can be derived by cdf(D)=$\int_{-\infty}^{b} f(D) dD$;

Step 2: Assume that $U^{(i)}$ obeys a uniform distribution within [0,1], which can be randomly collected from this interval and denoted as $U^{(i)}$~U(0,1).

Step 3: Substitute $U^{(i)}$ into the inverse function of the cumulative probability distribution cdf(D) to obtain random sample $D^{(i)}$, denoted by $D^{(i)} = cdf^{-1}(U^{(i)})$. Then, a dataset composed of n data points of $D^{(i)}$ is obtained.

Step 4: W_{ID} can be calculated by substituting n data points of $D^{(i)}$ into Eq. 10, and the P_{df} ($P_{df} = \frac{R_{ID}}{W_{ID}}$) corresponding to a specific AEP is determined. P_{df} represents the probability that the subsequent precipitation process may trigger debris flow for a certain AEP. Thus, the influence of the AEP on the occurrence probability of debris flows can be quantified.

3.5 Correlation analysis between numerical and observation results

The relationship between the AEP-P_{df} fitted through the observational data is used as a reference standard, and the correlation analysis method is used to verify the function of the AEP-P_{df} derived by Dens-ID. Correlation analysis is used to study the degree of linear correlation between variables, which is represented by correlation coefficient r:

$$r = \frac{\sum_{i=1}^{n}(x_i - \bar{x})(y_i - \bar{y})}{\sqrt{\sum_{i=1}^{n}(x_i - \bar{x})^2 \sum_{i=1}^{n}(y_i - \bar{y})^2}} \tag{12}$$

where x represents the P_{df} derived from the observed data, y represents the P_{df} derived from Dens-ID, $\bar{x}$ and $\bar{y}$ represent the averages, r represents the correlation coefficient, and n represents the number of samples. $|r| \geq 0.8$ can be regarded as a high correlation between two variables; $0.5 \leq |r| < 0.8$ represents a moderate correlation; $0.3 \leq |r| < 0.5$ represents a low correlation; and $|r| < 0.3$ indicates the degree of correlation between the two variables is weak and can be regarded as uncorrelated.

4 Results

4.1 ID threshold curves and warning zone closed by the derived curves

Dens-ID yields the upper and lower boundary lines of the ID threshold in each condition of a preset AEP, and these two boundary lines are characterized by different debris flow density and listed in Table 1.It can be seen from Table 1 that the maximum density corresponding to the ID threshold curve cannot reach 2.2, when AEP is less than15 mm. A small AEP indicates the supply rate of solid resources in JJG is far less than the runoff generation rate during a subsequent rainfall process. In this situation, runoff is dominated in the water-soil coupling process yielding a water-soil mixture with low density value.

Table 1 ID threshold curve database under different AEP

AEP (mm)	ID threshold curve function for JJG	
	1.2 g/cm^3	2.2 g/cm^3
10	$I_{1.2} = 19.85D^{-0.54}$ D∈[1, 269] (R^2 = 0.991)	**$I_{1.8}$**=15.85D$^{-0.48}$ D∈[1, 263] (R^2=0.990)
15	$I_{1.2}$= 21.69D$^{-0.55}$D∈[1, 236] (R^2=0.993)	**$I_{2.0}$**=16.10D$^{-0.50}$ D∈[1, 229] (R^2=0.995)
20	$I_{1.2}$=23.22D$^{-0.58}$D∈[1, 203] (R^2=0.996)	$I_{2.2}$=17.20D$^{-0.53}$ D∈[1, 192] (R^2=0.995)
25	$I_{1.2}$=24.47D$^{-0.60}$ D∈[1, 171] (R^2=0.997)	$I_{2.2}$=16.92D$^{-0.53}$ D∈[1, 160] (R^2=0.998)
30	$I_{1.2}$=26.24D$^{-0.64}$ D∈[1, 143] (R^2=0.996)	$I_{2.2}$= 18.09D$^{-0.57}$ D∈[1, 132] (R^2=0.995)
35	$I_{1.2}$=35.47D$^{-0.65}$ D∈[1, 123] (R^2=0.958)	$I_{2.2}$= 19.55D$^{-0.58}$ D∈[1, 112] (R^2=0.985)
40	$I_{1.2}$= 40.59D$^{-0.78}$ D∈[1, 103] (R^2=0.966)	$I_{2.2}$= 22.15D$^{-0.64}$ D∈[1, 92] (R^2=0.984)
45	$I_{1.2}$= 41.12D$^{-0.78}$ D∈[1, 83] (R^2=0.932)	$I_{2.2}$= 23.19D$^{-0.69}$ D∈[1, 72] (R^2=0.981)
50	$I_{1.2}$=41.26D$^{-0.86}$ D∈[1, 65] (R^2=0.981)	$I_{2.2}$= 23.50D$^{-0.74}$ D∈[1, 55] (R^2=0.980)
55	$I_{1.2}$=38.63D$^{-0.88}$ D∈[1, 53] (R^2=0.950)	$I_{2.2}$= 23.31D$^{-0.70}$ D∈[1, 42] (R^2=0.932)
60	$I_{1.2}$= 31.49D$^{-0.92}$ D∈[1, 40] (R^2=0.992)	$I_{2.2}$= 20.73D$^{-0.86}$ D∈[1, 30] (R^2=0.977)
65	$I_{1.2}$= 29.14D$^{-0.95}$ D∈[1, 32] (R^2=0.957)	$I_{2.2}$= 18.10D$^{-0.91}$ D∈[1, 22] (R^2=0.893)
70	$I_{1.2}$= 23.05D$^{-0.96}$ D∈[1, 25] (R^2=0.998)	$I_{2.2}$= 13.04D$^{-0.93}$ D∈[1, 15] (R^2=0.995)
75	$I_{1.2}$= 21.13D$^{-0.97}$ D∈[1, 22] (R^2=0.994)	$I_{2.2}$=10.90D$^{-0.95}$ D∈[1, 12] (R^2=0.995)
80	$I_{1.2}$= 18.72D$^{-0.98}$ D∈[1, 20] (R^2=0.997)	$I_{2.2}$= 9.96D$^{-0.95}$ D∈[1, 11] (R^2=0.999)
85	$I_{1.2}$= 18.47D$^{-0.99}$ D∈[1, 18] (R^2=0.999)	$I_{2.2}$= 8.17D$^{-0.95}$ D∈[1, 9] (R^2=0.999)

284   Under the condition of AEP < 10 mm, Dens-ID cannot derive the threshold curve

285   corresponding to even the minimum density value of 1.2 g/cm^3, which indicates that the subsequent

286   rainfall can hardly trigger debris flow JJG. Table 1 also shows that the AEP ranging from 10 to 85

287   mm can significantly affect the ID threshold curve, because the parameters including α and β

288   regularly respond to the change in AEP.
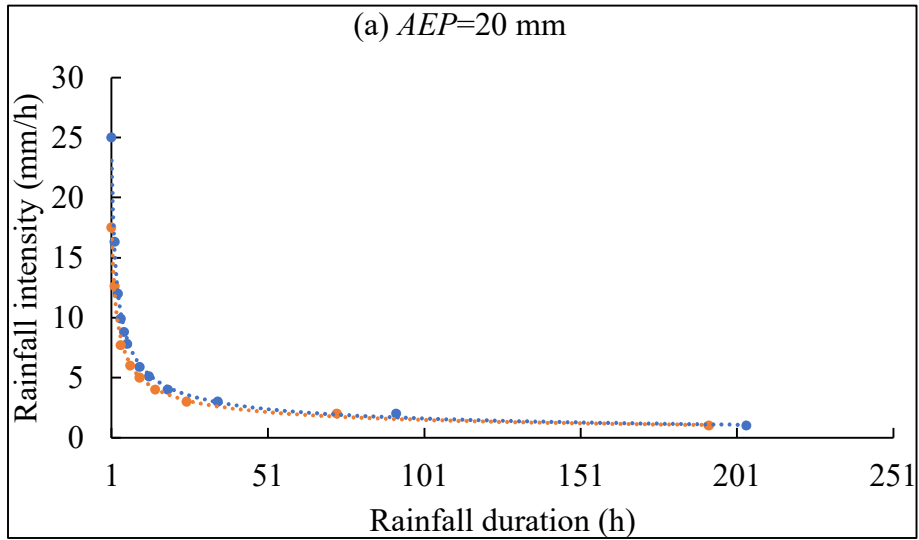
289

290
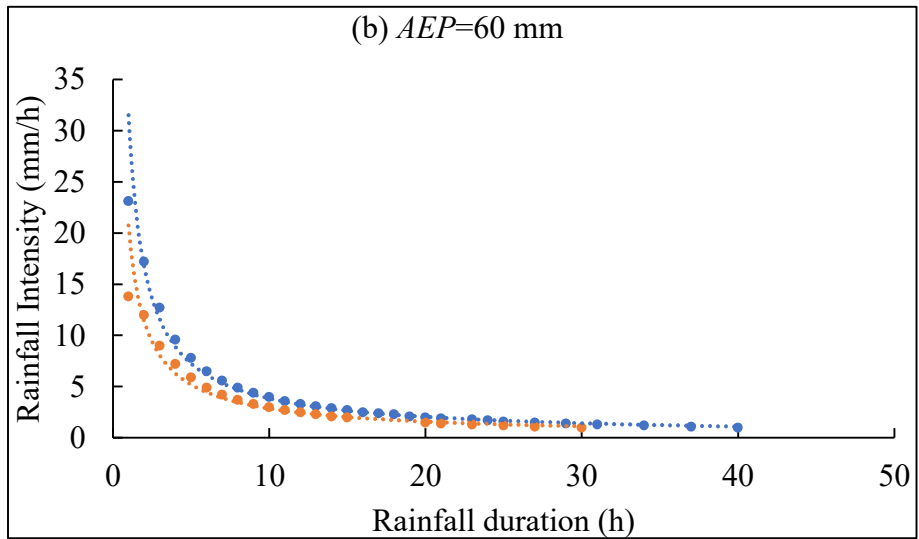
291

292
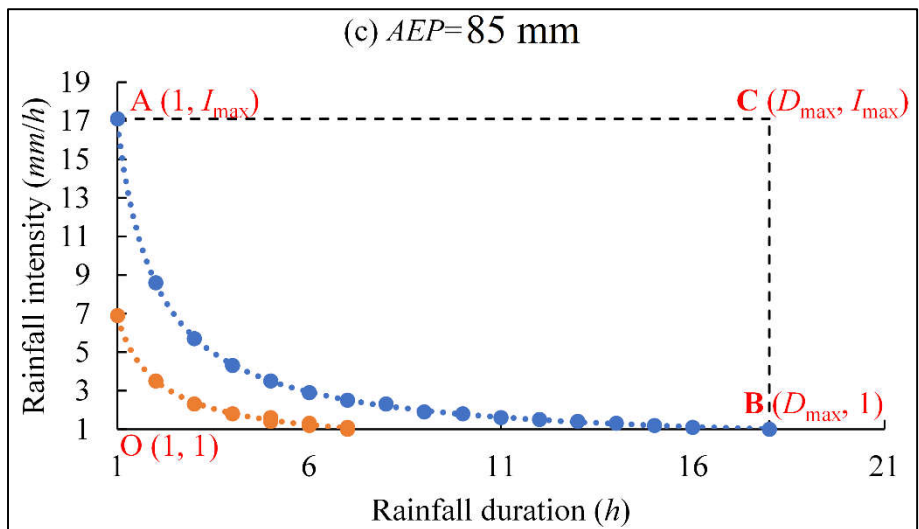
293

294   Fig.2 ID threshold curves derived by Dens-ID (the blue dotted line corresponds to 1.2 g/cm³, and

295   the orange dotted line corresponds to 2.2 g/cm^3)

296   There are two ID threshold curves in each subplot of Fig. 2, which correspond to 1.2 g/cm^3 and

297   2.2 g/cm^3, respectively. Because the debris flow density in JJG varies within a certain range from

298   1.2–2.3 g/cm^3, the two ID threshold curves shown in each subplot can be regarded as the upper and

299   lower boundary lines for determining the occurrence of debris flow (Zhang et al., 2020). Within the

300   ID coordinate system, the two derived curves together with the I- and D-axes delineate a closed area

301   shown in Fig.2c. Any subsequence rainfall represented by the combination of I and D falling into

302   W_{ID} may trigger a debris flow. As shown in each subplot, the threshold curve can be represented by

303   the power function I=αD^β. The variation intervals of the independent (D) and dependent (I) variables

304   of the power function are [1, D_{max}] and [1, I_{max}], respectively, where D_{max} represents the rainfall

305   duration required to trigger debris flow when I= 1 mm/h, and I_{max} represents the rainfall intensity

306   required for debris flow formation for D=1 h. As shown in Fig.2c, independent variable D and

307   dependent variable I can delineate a larger rectangular area (AOBC) in the ID plane than W_{ID}, which

308   is denoted as R_{ID}. The coverage area of R_{ID} is much larger than that of W_{ID} indicating that the

309   proportion of rainfall conditions that can trigger debris flows is low. Therefore, even for AEP=85

310   mm, the occurrence probability of debris flows remains low. As shown in each subplot, each AEP

311   corresponds to a different W_{ID} and R_{ID}, which provides basic data for the quantitative evaluation of

312   the effect of different AEPs on the occurrence probability of debris flows.

313   **4.2 Occurrence probability of debris flow under different AEP**

314   Based on the Monte Carlo method of calculating the definite integral, it is necessary to explore

315   the probability density function of rainfall duration (D) to calculate the occurrence probability of

316   debris flow under different AEP conditions. For the 1094 rainfall events listed in Appendix 1, we

317   found that the probability distribution of rainfall duration D in JJG can be described by a power

318   function (Fig. 3). As shown in Fig.3, the number of samples with D<1 accounted for 37.7%, 1<D<3

319   for 23.5%, 3<D<5 for 14.7%, and 5<D<10 for 16.9%; the number of rainfall events with D

320   exceeding 10 h accounted for only 6.7%.
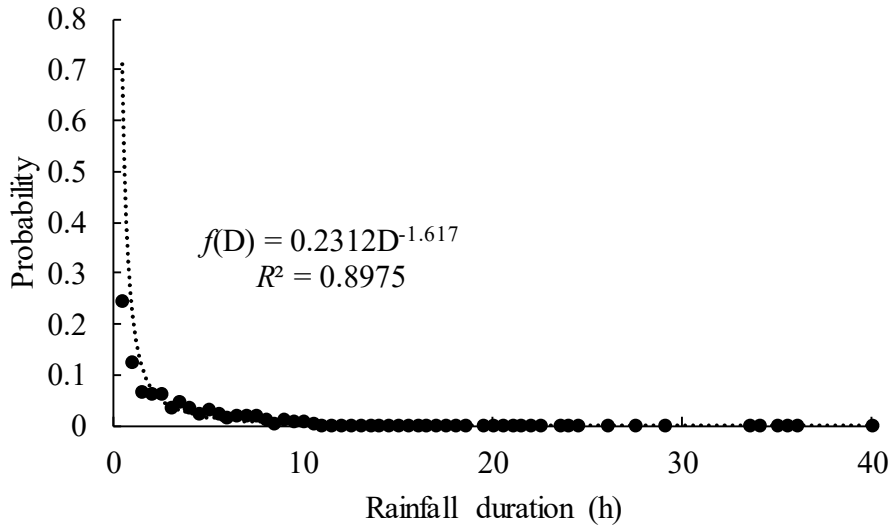
321

322   Fig. 3 Probability density function of f(D)

323   Based on the probability density distribution function f(D)=0.2312D$^{-1.617}$, the cumulative

324   probability function cdf(D) can be obtained through integration. In cdf(D), denoted as Eq. 13, the

325   integration constant C needs to be determined.

$$cdf(D)= \int_{-\infty}^{D} f(D)dD =-0.3747*D^{-0.617}+C \qquad (13)$$

327   The range of 0–40 h is evenly divided into 56 statistical intervals (the second column in

328   Appendix 2, titled "appendix 2-f(D)and CFD(D). xlsx"), and each statistical interval is separated by

329   0.5 h. The proportion of the sample size in each interval among the 1094 samples can be calculated

330   and listed in the second column in Appendix 2; the cumulative proportion that increases with D is

331   also derived and listed in the third column in Appendix 2. The data in the first and third columns of

332   Appendix 2 are substituted into Eq. 13 to calculate C. The results show that C increases with D but

333   gradually stabilizes at approximately 1.04 (the fifth column in Appendix 2). Therefore, C is set to

334   1.04.

335   Based on the process of calculating P_{df} under different AEP conditions in Section 3.4, the P_{df}

336   corresponding to each AEP in Table 1 is obtained, and the function $P_{df} = f(AEP)$ for describing

337   their relationship has been fitted using the AEP and P_{df} data.

338
$$\begin{cases} P_{df} = 0 & 0 < AEP < 10 \\ P_{df} = 0.3442e^{0.04\ 5\ AEP} & 10 \le AEP \le 85 \end{cases} \tag{14}$$

339   As shown in Eq.14, $P_{df} = f(AEP)$ is a piecewise function. The evolution of P_{df} with AEP

340   variation can be divided into two stages (Fig. 4). Two key issues must be stated before discussing

341   the two stages in depth: (1) Based on the calculation results of the Dens-ID model, an upper limit

342   volume of the rainfall-induced solid material supply is derived in JJG, which is the basic condition

343   for determining the scale of debris flow in JJG (Zhang et al., 2020). (2) Based on the principle of

344   water balance, AEP is defined as the rainfall that is preserved in the soil before the triggering rainfall

345   process (Kohler and Linsley, 1951); field observations in JJG show that the AEP is positively

346   correlated with the soil water content (Cui et al., 2007), and the field observations of the Liudaogou

347   catchment in the northern Loess Plateau of China have the same result (Zhu and Shao, 2008);

348   therefore, the AEP is typically used to estimate soil water content (Crozier, 1986; Chen et al., 2018;

349   Zhao et al., 2019b). The water soil content before the triggering rainfall process can be characterized

350   by AEP (Thomas et al., 2019; Schoener and Stone, 2020).
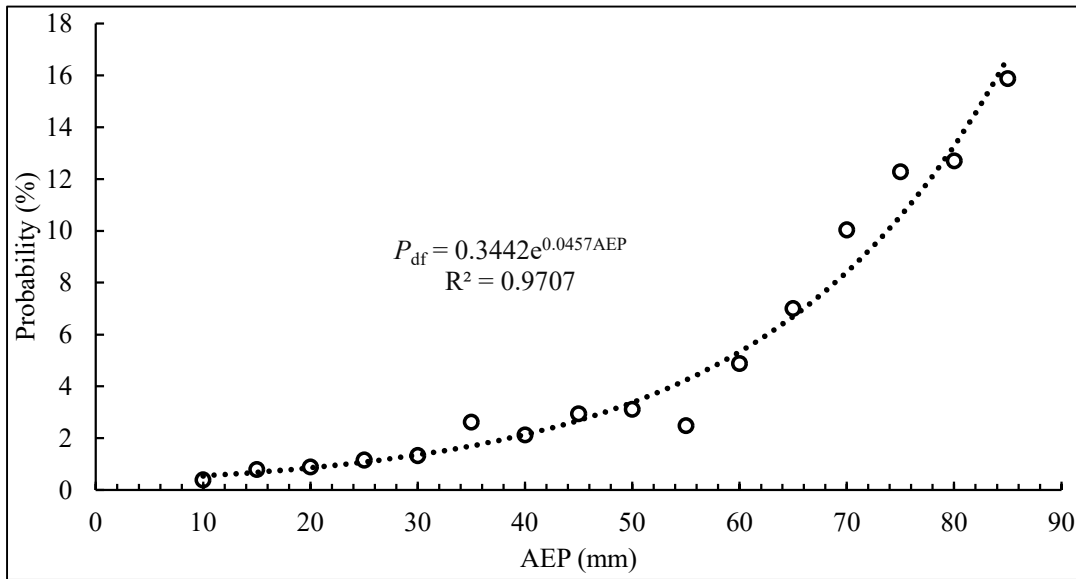
351

352   Fig.4 Relationship of P_{df} and AEP derived from Dens-ID

353   Stage 1: The probability of debris flow occurrence in JJG is equal to 0 when the AEP is < 10

354   mm. Dens-ID estimates the solid material volume by simulating rainfall-induced shallow landslides.

355   According to Eq. 4, the key hydrological process that triggers shallow landslides is the continuous

356   increase in soil water content caused by rainfall infiltration. The increase in soil moisture content

357   reduces soil matrix suction and eventually contributes to shallow landslides. The soil water content

358   of the loose soil mass in JJG is low when the AEP < 10 mm (Long et al., 2020), and a long duration

359   of rainfall infiltration is needed to increase the soil water content. However, based on the infiltration

360   border of Dens-ID (Eq. 1), limited by the infiltration capacity of the topsoil in JJG, the portion of

361   precipitation that exceeds the infiltration capacity is be converted into runoff; therefore, when the

362   water content of the soil layer in JJG is low, the surface runoff can be rapidly generated. Therefore,

363   the runoff generation rate can be much higher than the supply rate of solid material in the condition

364   of AEP < 10 mm. In this hydrological scenario, Dens-ID determines that even a soil-water mixture

365   with a density of 1.2 g/cm^3 is difficult to generate in JJG; thus, the probability of debris flow is 0.

366   Stage 2: When AEP varies within the interval of 10 mm-85mm, the subsequent rainfall is

367 capable of triggering debris flow in JJG. Compared to AEP < 10 mm in Stage 1, the soil water

368 content within JJG increased significantly. Therefore, the solid material from shallow landslides can

369 be immediately ready without a long rainfall infiltration duration, and a large water content of

370 topsoil is beneficial to the rapid generation of runoff (Jones et al., 2017; Hirschberg et al., 2021).

371 When there is a sufficient supply of solid material and runoff, the probability of debris flow

372 occurrence in Stage 2 is significantly increased by the increasing AEP. The relationship between

373 $P_{df} \sim AEP$ can be described by an exponential function of $P_{df}=0.3442e^{0.0457AEP}$. The exponential

374 function and its boundary show that the increasing tendency of P_{df} is a little sluggish before AEP is

375 equal to 50 mm. The occurrence probability of debris flow in JJG is only 15.88% even when AEP

376 is equal to 85 mm.

377 **5 Discussions**

378 **5.1 Correlation analysis of the two curves derived from Dens-ID and observation data**

379   The AEP in Appendix 1 varied from 0–87.9 mm, according to this range, we can test the

380 reasonability of the relationship between $P_{df} \sim AEP$ shown in Fig. 4. We introduce how to use the

381 rainfall and debris flow data recorded in Appendix 1 to calculate P_{df}: (1) The original AEP value is

382 rounded to one decimal place, and the rounded AEP are listed in the 8th column of Appendix 1,

383 which were sorted from largest to smallest; (2) the maximum AEP_i was set to 85 mm, and [AEP_i,

384 AEP_i-5] was used as the search window to collect the rainfall events and debris flow events; and (3)

385 we count the number of debris flow events N_{df} and the number of rainfall events N_{rain} in each search

386 window and then calculate $P_{df}=N_{df}/N_{rain}$. Based on the above steps, the collected data and calculated

387 P_{df} are listed in Table 2. As shown in Table 2, a positive correlation between the probability of debris

388   flow occurrence and AEP in JJG was determined. When AEP < 10 mm, a total of 205 rainfall

389   processes were recorded; however, no debris flow events were observed, and the debris flow

390   occurrence probability was 0, which is consistent with the results of Stage 1 derived from Dens-ID.

391   Table 2 Collected and calculated P_{df} in each search window

	Field observation data and calculated P_{df}										
AEP	10	15	20	25	30	35	40	45	50	75	80
N_{df}	0	3	2	7	7	4	4	5	3	1	1
N_{rain}	205	133	111	127	124	106	106	49	31	8	5
P_{df} (%)	0	2.3	1.8	5.5	5.6	3.8	3.8	10.2	9.7	12.5	20

392   Based on P_{df} and AEP listed in Table 2, their relationship can be described by the exponential

393   function denoted as $P_{df} = 1.5917e^{0.03 \, 1AEP}$, which is similar to Eq.14 drawn in Fig.4. The two

394   curves were nearly parallel. Eq. 12 was used to analyze the correlation of the two curves, and r is

395   equal to 0.93, suggesting they have a very high correlation. Therefore, the function of $P_{df} =$

396    $f(AEP)$ derived from Dens-ID, which is used to describe the evolution trend of debris flow

397   occurrence probability with AEP variation, is reasonable.
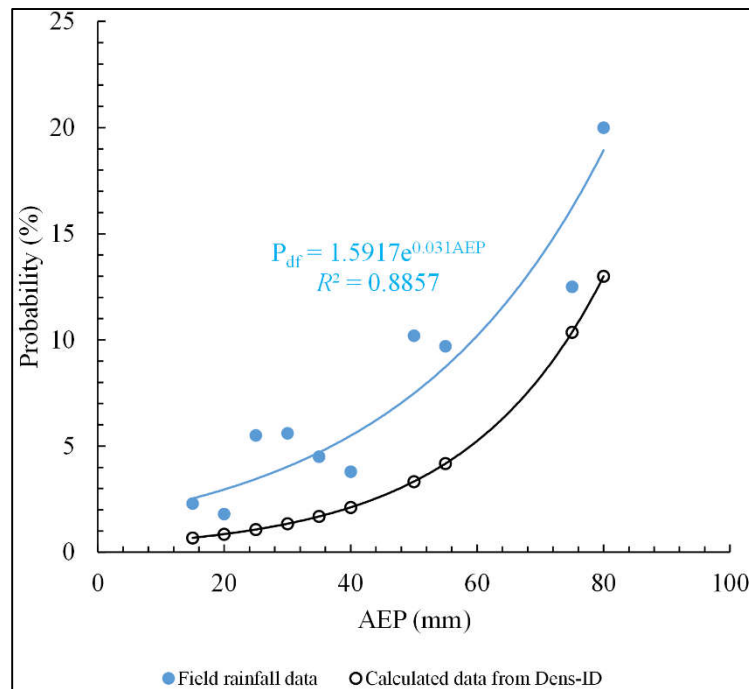
398

399   Fig.5 Relationship of AEP and P_{df} obtained from field observation data and Dens-ID model (the blue line is

400   derived from field observation data, and the black line is derived from Dens-ID)

401   We can also see from Fig.5 that although the variation tendencies of the two curves are

402 consistent, a significant bias is existed between them. Basically, the probability value derived from

403 the field observation data is larger than that from the Dens-ID model in the condition of a given

404 AEP. As shown in Fig.5, the blue line fitted through the observation data is above the black line

405 derived from Dens-ID, indicating that Dens-ID underestimated the probability of debris flow

406 occurrence if the observation data were used as the reference. Taking the probability value in the 6th

407 row of Table 2 as references, the error of the Eq.14 was calculated using the AEP in Table 2 as inputs

408 and listed in Table 3.

409   Table 3 Error estimation on the Eq. 14

AEP	15	20	25	30	35	40	45	50	75	80
Error	0.70	0.53	0.81	0.76	0.63	0.44	0.67	0.57	0.17	0.35

410   It can be seen that very large bias of Eq.12 is listed in Table 2. However, we cannot conclude

411 that there is a precision problem in the calculation results of the Dens-ID. Because (1) Although

412 1094 rainfall processes and 37 debris flow events are the field observation data, there are many

413 uncertain factors in Eq. 7 for calculating AEP using these rainfall data (Kim et al., 2021), such as

414 the subjectivity existing in K and n of Eq. 7, which render uncertainty in the calculated AEP. In this

415 case, if the data in Appendix 1 are used as the real value for evaluating the precision of Dens-ID,

416 the error evaluation result may be unfair to Dens-ID. In this case, it is unfair to evaluate the Dens-

417 ID error by using the calculated AEP in Appendix 1 as the true value. However, this uncertainty can

418 show consistent directional deviations because of the fixed values of K and n in Eq.7; therefore, the

419 uncertainty has no effect on the correlation analysis. (2) To establish the functional relationship

420 between P_{df}-AEP, many rainfall scenarios were simulated using the Dens-ID model. Dens-ID

421 simulated 3376, 3182, 2677, and 2677 rainfall processes with AEP = 20, 40, 45, and 50 mm,

422 respectively. The total number of simulated rainfall processes was significantly larger than that of

423 the 1094 observed rainfall events. The collected 1094 rainfall events still cannot fully reflect all

424 rainfall conditions in nature; that is, the amount of the observed 1094 rainfall data is still inadequate

425 when used as the denominator for calculating the probability of debris flow occurrence in JJG.

426 Therefore, the P_{df} calculated using the field observation data may be generally higher than that

427 calculated using Dens-ID. With the accumulation of rainfall observation data of JJG, it is believed

428 that the Pdf derived from field observation data will gradually decrease until it is close to the

429 calculated value of Dens-ID model. (3) Dens-ID cannot fully and accurately describe the formation

430 process of the debris flow in JJG because of the simplification in theory and boundaries. Dens-ID

431 is also affected by the accuracy of the input parameters (Zhang et al., 2020), which may eventually

432 lead to deviations between the simulation results and field observations.

433 5.2 Potential application and limitation

434   Deriving a quantified functional relationship of P_{df} and AEP would be more conducive to

435 examining the correspondence between these two parameters. Using mathematical physics method,

436 the function of $P_{df} = f(AEP)$ was firstly derived which can help us to learn more from the derived

437 $P_{df} = f(AEP)$.

438   Firstly, AEP is indeed an important factor affecting debris flow. Generally, there is the

439 following consensus in the field of debris flow: the greater the AEP, the higher the probability (P_{df})

440 of subsequent rainfall triggering the debris flow (De Vita et al., 2000; Bel et al., 2017). However,

441 this fuzzy qualitative description cannot explain the influence degree of AEP on the probability of

442   debris flow induced by subsequent rainfall. It can be seen from $P_{df} = f(AEP)$ that there are two

443   key value nodes of AEP affecting P$_{df}$: (1) point 10 mm:the case of AEP < 10 mm indicates that

444   any subsequent rainfall cannot trigger debris flow in JJG. Because the supply rate of solid material

445   is much lower than the runoff generation rate during subsequent rainfall in JJG, the water-soil

446   mixture within tends to be a hyperconcentrated flow rather than a debris flow (Long et al., 2020);

447   (2) Point 50 mm: the case of 10 mm≤AEP≤50 mm means that the soil water content increases

448   significantly compared to AEP < 10 mm, but a necessary infiltration time to increase it to the critical

449   state for triggering shallow landslides is still required. Therefore, limited by the supply rate of the

450   solid material, the increasing rate of P_{df} is sluggish. The case of 50 mm<AEP≤85 mm represents

451   the soil water content is relatively larger, the solid material from shallow landslides can be

452   immediately ready without a long rainfall infiltration duration, and a large soil water content of

453   topsoil is beneficial to the rapid generation of runoff (Jones et al., 2017; Hirschberg et al., 2021).

454   When there is a sufficient supply of provenance and runoff, the probability of debris flow occurrence

455   in this subprocess is significantly enhanced by the increasing AEP.

456   Secondly, Rainfall-induced debris flow is a small probability event compared with the rainfall

457   frequency in nature. JJG is well-known due to its high-frequency debris flow event. However, the

458   formation probability of debris flow in JJG induced by subsequence rainfall is only 15.88% even

459   the AEP reaches to 85 mm. Therefore, debris flow induced by rainfall in JJG is a small probability

460   event compared with the rainfall frequency. The figure of 15.88% means that the efficiency of rain-

461   induced debris flow is extremely low, which also indicates that the formation of debris flow is an

462   extremely complex physical process, in which rainfall is only one of the motivating factors, and

463   there are other more important internal factors affecting the formation of debris flow, such as

464   topography, source recharge and fluid characteristics of debris flow (Zhang et al., 2020). Thirdly, in

465   practical application, when the AEP in JJG is calculated according to Eq.7, the derived exponential

466   function can help us to assess the probability of debris flow in JJG triggered by subsequent rainfall,

467   according to which debris flow warning information can be issued in advance to provide technical

468   support for disaster prevention and reduction.

469   Our study also has its own limitations and needs to be listed for providing directions for

470   subsequent investigation. (1) Long-term observation data should be used to deduce the functions of

471    $P_{df} = f(AEP)$, however, the number of debris flow gullies with long-term observational data

472   worldwide is less than 10 (Hürlimann et al., 2019), accordingly, the function of $P_{df} = f(AEP)$

473   cannot yet be derived in other debris-flow gullies. (2) Dens-ID model assumes that the solid

474   material mainly comes from shallow landslides. However, the formation mechanism and solid

475   source supply mode of runoff-induced debris flow are different. Therefore, the functional of $P_{df} =$

476    $f(AEP)$for runoff-induced debris flow still needs to be studied with the help of other physical

477   models. (3) The calculation result of $P_{df} = f(AEP)$ derived from Dens-ID model has a large bias

478   from the observation data, the authors think that the main reason is insufficient field observation

479   data especially inadequate rainfall data. Basically, even for high-frequency debris flow gullies like

480   JJG, the success rate of debris flow induced by rainfall is still very low. Continuous increase of

481   rainfall and debris flow observation data will make the growth rate of Nrain in Table 2 much higher

482   than that of Ndf. Therefore, with the accumulation of rainfall observation data of JJG, it is believed

483   that the P_{df} derived from field observation data will gradually decrease until it is close to the

484   calculated result of Dens-ID model. Therefore, the authors will continue to collect field observation

485   data of JJG in the later period, and constantly verify the accuracy of Eq.14 derived from Dens-ID.

486

5 Conclusions

The Dens-ID model and Monte Carlo integral equation is used to derive function of $P_{df} = f(AEP)$. The functional relationship is verified using a large amount of field observation data from JJG. The following conclusions are drawn as follows.

The positive relationship between P_{df} and AEP is now described by a clear mathematical equation in this study. the effective range of AEP that can affect debris flow formation verifies within 10–85 mm. Based on the simulation results, the probability of debris flow occurrence in JJG is 0 in the condition of AEP < 10 mm, and the relationship between P_{df} and AEP can be described by an exponential function when 10 mm≤AEP≤85 mm. The plausibility of the first two evolution stages of the P_{df}-AEP piecewise function is effectively confirmed by the field observation data because the P_{df}-AEP relationship obtained from field observation data is highly correlated with the simulation results of Dens-ID. However, the reasonability of the last two stages of the P_{df}-AEP piecewise function cannot be tested because of the lack of field observation data, and the errors of the P_{df}-AEP piecewise function cannot be verified because of the uncertainty of the AEP derived from the observation rainfall data.

This study mathematically confirms that "the greater the AEP, the higher the probability of subsequent rainfall triggering debris flow" and quantifies this qualitative conclusion using piecewise functions. This can effectively reveal the essential relationship between the two natural events of rainfall and debris flow, quantitatively describe the impact of different AEPs on the probability of debris flow occurrence, and provide key technical support for the early warning of debris flows.

Acknowledgement:

This work was supported by the National Key Research and Development Program of China (2023YFC3007205), the West Light Foundation of The Chinese Academy of Science, National Natural Science Foundation of China (No. 42271013, No. 42001100), Project of the Department of Science and Technology of Sichuan Province (No. 2023ZHCG0012).

References

Abraham, M.T., Satyan, N., Rosi, A., Pradhan, B., Segoni, S.: Usage of antecedent soil moisture for improving the performance of rainfall thresholds for landslide early warning. Catena, 200, 105147, 2021.

Abraham, M.T., Satyam, N., Pradhan, B., Alamri, A.M.: Forecasting of landslides using rainfall severity and soil wetness: A probabilistic approach for Darjeeling Himalayas. Water (Switzerland) 12, 1–19, 2020.

Adams, B., Fraser, H., Howard, C., Hanafy, M.: Meteorological data analysis for drainage system design. J. Environ. Eng. 112, 1986.

Albert, G.E.: A general theory of stochastic estimates of the Neumann series for solution of certain Fredholm integral equations and related series, in: M.A. Meyer (Ed.), Symposium of Monte Carlo Methods, Wiley, New York, 1956.

Bel, C., Liébault, F., Navratil O., Eckert N., Bellot H., Fontaine, F., Laigle, D.: Rainfall control of debris-flow triggering in the Réal Torrent, Southern French Prealphs, 291, 17-32, 2017.

Bennett, G.L., Molnar, P., Mcardell, B.W., Burlando, P.: A probabilistic sediment cascade model of sediment transfer in the Illgraben. Water Resources Research, 50, 1225-1244, 2014.

Bernard, M., Gregoretti, C.: The use of rain gauge measurements and radar data for the model-based prediction of runoff-generated debris flow occurrence in early warning systems. Water Resources

530   Research, 57, e2020WR027893, 2021.

531   Berti, M., Simoni, A.: Experimental evidences and numerical modelling of debris flow initiated by

532   channel runoff. Landslides, 3, 171-182, 2005.

533   Calvo, B., Savi, F.: A real-world application of Monte Carlo procedure for debris flow risk

534   assessment, Computers and Geosciences, 35(5), 967-977, 2009.

535   Castillo, V.M., Gómez-Plaza, A., Martínez-Mena, M.: The role of antecedent soil water content in

536   the runoff response of semiarid catchments: a simulation approach. Journal of Hydrology, 284,

537   114-130, 2003.

538   Chen, C.W., Oguchi, T., Chen, H., Lin, G.W. Estimation of the antecedent rainfall period for mass

539   movements in Taiwan, Environmental Earth Sciences, 77, 184, 2018.

540   Chen, C.W., Saito, H., Oguchi, T.: Analyzing rainfall-induced mass movements in Taiwan using the

541   soil water index, Landslides, 14, 1031-1041, 2017.

542   Coe, J.A., Kinner, D.A., Godt, J.W. Initiation conditions for debris flows generated by runoff at

543   Chalk Cliffs, central Colorado. Geomorphology, 3, 270-297, 2008.

544   Crozier, M.J.: Landslides: causes, consequences & environment. Croom Helm, London, p 25, 1986.

545   Cui, P., Zhu, Y.Y., Chen, J., Han, Y.S., Liu, H.J.: Relationships between antecedent rainfall and

546   debris flows in Jiangjia Ravine, China. In: Chen & Major, eds., Debris-Flow Hazards Mitigation:

547   Mechanics, Prediction, and Assessment, Millpress, Netherlands, 3-10, 2007.

548   De Vita, P.: Fenomeni d'instabilita` delle coperture piroclastiche dei Monti Lattari, di Sarno e di

549   Salerno (Campania) ed analisi degli eventi pluviometrici determinanti. Quad. Geol. Appl., 7, 213–

550   239, 2000.

551   Donovan, I.P., Santi, P.M. A probabilistic approach to post-wildfire debris-flow volume modeling,

552   Landslides, 14(4): 1345-1360, 2017.

553   Fiorillo, F., Wilson, R.C. Rainfall induced debris flows in pyroclastic deposits, Campania (southern

554   Italy). Engineering Geology, 75, 263-289, 2004.

555   Gabet, E.J., Mudd, S.M.: The mobilization of debris flows from shallow landslides. Geomorphology

556   1, 207-218, 2006.

557   Han, Z., Chen, G.Q., Li, Y.G., He, Y.: Assessing entrainment of bed material in a debris-flow event:

558   a theoretical approach incorporating Monte Carlo method: Assessing Entrainment of Bed

559   Material by Debris Flow, Earth surface processes and landforms, 40(14): 1877-1890, 2015.

560   Hirschberg, J., Badoux, A., McArdell, B.W., Leonarduzzi, E., Molnar, P.: Evaluating methods for

561   debris-flow prediction based on rainfall in an Alpine catchment. Nat. Hazards Earth Syst. Sci.,

562   21, 2773-2789, 2021.

563   Hong, M., Kim, J., Jeong, S.: Rainfall intensity-duration thresholds for landslide prediction in South

564   Korea by considering the effects of antecedent rainfall. Landslides, 15, 523–534, 2018.

565   Hu, W., Xu, Q., Wang, G.H., van Asch, T.W.J., Hicher, P.Y.: Sensitivity of the initiation of debris

566   flow to initial soil moisture. Landslides 12, 1139–1145, 2015.

567   Huang, C.H.: Critical rainfall for typhoon-induced debris flows in the Western Foothills, Taiwan.

568   Geomorphology, 185, 87-95, 2013.

569   Hürlimann, M. Coviello, V., Bel, C., Guo, X.J., Berti, M., Graf, C., Hübl, J., Miyata, S., Smith, J.B.,

570   Yin, H.Y.: Debris-flow monitoring and warning, Review and examples. Earth-Science Reviews,

571   199, 102981, 2019.

572   Iverson, R. M., Reid, M. E., LaHusen, R. G.: Debris Flow Mobilization from Landslides. Annu. Rev.

573   Earth Planet, 25: 85-138, 1997.

574   Jones, R., Thomas, R.E., Peakall, J., Manville, V.: Rainfall-runoff properties of tephra: Simulated

575   effects of grain-size and antecedent rainfall. Geomorphology, 282, 39-51, 2017.

576   Kim, S.W., Chun, K.W., Kim, M., Catani, F., Choi, B., Seo, J.: Effect of antecedent rainfall

577   conditions and their variations on shallow landslide-triggering rainfall thresholds in South Korea.

578   Landslides, 18, 569-582, 2021.

579   Kohler, M.A., Linsley, R.K.: Predicting the runoff from Storm Rainfall. US Department of

580   Commerce, Weather Bureau, Washington, D.C, 1951.

581   Le Bissonnais, Y., Renaux, B., Delouche, H. Interactions between soil properties and moisture

582   content in crust formation, runoff and interrill erosion from tilled loess soils. Catena, 25(1), 33-

583   46, 1995.

584   Li, L., Zhang, S.X., Li, S.H., Qiang, Y., Zheng, Z., Zhao, D.S.: Debris Flow Risk Assessment

585   Method Based on Combination Weight of Probability Analysis, Advances in civil engineering,

586   2021, 1-12, 2021.

587   Liu, D.L., Zhang, S.J., Yang, H.J., Zhao, L.Q., Jiang, Y.H., Tang, D., Leng, X.P.: Application and

588   analysis of debris-flow early warning system in Wenchuan earthquake-affected area. Nat. Hazards

589   Earth Syst. Sci., 16, 483-496, 2016.

590   Liu, X.L., Wang, F., Nawnit, K., Lv, X.F., Wang, S.J. Experimental study on debris flow initiation.

591   Bulletin of Engineering Geology and the Environment, 79, 1565-1580, 2020.

592   Long, K., Zhang, S.J., Wei, F.Q., Hu, K.H., Zhang, Q., Luo, Y. A hydrology-process based method

593   for correlating debris flow density to rainfall parameter and its application on debris flow

594   prediction. Journal of Hydrology, 589, 125124, 2020.

595   Luk, S.H.: Effect of antecedent soil moisture content on rainwash erosion. Catena, 12, 129-139,

1985.

Marra, F., Destro, E., Nikolopoulos, E.I., Zoccatelli, D., Creutin, J.D., Guzzetti, F., Borga, M.: Impact of rainfall spatial aggregation on the identification of debris flow occurrence thresholds. Hydrol. Earth Syst. Sci., 21, 4525-4532, 2017.

Paola, F.De., Risi, R.De., Crescenzo, G. Di, Giugni, M., Santo, A., Speranza, G.: Probabilistic Assessment of Debris Flow Peak Discharge by Monte Carlo Simulation, Journal of Risk and Uncertainty in Engineering Systems, Part A: Civil Engineering, 3(1), A4015002, 2017.

Papa, M.N., Medina, V., Ciervo, F., Bateman, A.: Derivation of critical rainfall thresholds for shallow landslides as a tool for debris flow early warning systems. Hydrol. Earth Syst. Sci. 17, 4095-4107, 2013.

Peres, D.J., Cancelliere, A.: Derivation and evaluation of landslide-triggering thresholds by a Monte Carlo approach. Hydrol. Earth Syst. Sci., 18, 4913-4931, 2014.

Peres, D.J., Cancelliere, A.: Modeling impacts of climate change on return period of landslide triggering. Journal of Hydrology, 567, 420-434, 2018.

Richards, L.A. Capillary condition of liquids in porous mediums. Physics 1, 318–333, 1931.

Schoener, G., Stone, M.C.: Monitoring soil moisture at the catchment scale-A novel approach combing antecedent precipitation index and rader-derived rainfall data, Journal of Hydrology, 589, 125155, 2020.

Segoni, S., Piciullo, L., Gariano, S.L.: A review of the recent literature on rainfall thresholds for landslide occurrence, Landslides, 15:1483-1501, 2018b.

Segoni, S., Rosi, A., Lagomarsino, D., Fanti, R., Casagli, N.: Brief communication: Using averaged soil moisture estimates to improve the performances of a regionalscale landslide early warning

618   system. Nat. Hazards Earth Syst. Sci. 18, 807–812, 2018a.

619   Senthilkumar, V., Chandrasekaran, S.S., Maji, V.B.: Geotechnical characterization and analysis of

620   rainfall-induced 2009 landslide at Marappalam area of Nilgiris district, Tamil Nadu state, India.

621   Landslides, 14, 1803-1814, 2017.

622   Tang, H., Mcguire, L.A., Kean, J.W., Smith, J.B.: The impact of sediment supply on the initiation

623   and magnitude of runoff-generated debris flows. Geophysical Research Letters, 47,

624   e2020GL087643, 2020.

625   Thomas, M.A., Collins, B.D., Mirus, B.B.: Assessing the feasibility of satellite-based thresholds for

626   hydrologically driven landsliding. Water Resource Research, 55, 9006-9023, 2019.

627   Tisdall, A.: Antecedent soil moisture and its relation to infiltration. Aust. J. Agric. Res., 2 (3), 342–

628   348, 1951.

629   Van Genuchten, M.: A closed form equation for predicting the hydraulic conductivity of unsaturated

630   soils. Soil Sci. Soc. Am. J. 44, 892–898, 1980.

631   Wei, F.Q., Hu, K.H., Zhang, J., Jiang, Y.H., Chen, J.: Determination of effective antecedent rainfall

632   for debris flow forecast based on soil moisture content observation in Jiangjia Gully, China. In:

633   DeWrachien, D., Brebbia, C.A., Lenzi, M.A., eds., Monitoring, Simulation, Prevention and

634   Remediation of dense debris flows II. WIT Transactions on Engineering Sciences, England. 13-

635   22, 2008.

636   Yan, Z.Z., Hong, Z.M.: Using the Monte Carlo method to solve integral equations using a modified

637   control variate. Applied mathematics and computation, 242,764-777, 2014.

638 Yang, H.J., Zhang, S.J., Hu, K.H., Wei, F.Q., Wang, K., Liu S.: Field observation of debris flow

639   activities in the initiation area of Jiangjia Gully, Yunnan Province, China, Journal of Mountain

640   Science, 19(6): 1602-1617, 2022.

641 Zeng, Q.L., Yue, Z.Q., Yang, Z.F., Zhang, X.J.: A case study of long-term field performance of

642   check-dams in mitigation of soil erosion in Jiangjia stream, China. Environ Geol 58:897–911,

643   2009.

644 Zhang, S.J., Xu, C.X., Wei, F.Q., Hu, K.H., Xu, H., Zhao, L.Q., Zhang, G.P.: A physics-based model

645   to derive rainfall intensity-duration threshold for debris flow. Geomorphology, 351, 106930, 2020.

646 Zhang, S.J., Yang, H.J., Wei, F.Q., Jiang, Y.H., Liu, D.L.: A model of debris flow forecast based on

647   the water-soil coupling mechanism. Journal of Mountain Science, 25, 757-763, 2014.

648 Zhang, S.J., Xia, M.Y., Li, L., Yang, H.J., Liu, D.L., Wei, F.Q.: Quantify the effect of antecedent

649   effective precipitation on rainfall intensity-duration threshold of debris flow. Landslides, 20,

650   1719-1730, 2023.

651 Zhao, B.R., Dai, Q., Han, D.W., Dai, H.C., Mao, J.Q., Zhuo, L.: Probabilistic thresholds for

652   landslides warning by integrating soil moisture conditions with rainfall thresholds. Journal of

653   Hydrology, 574, 276-287, 2019a.

654 Zhao, B.R., Dai, Q., Han, D., Dai, H., Mao, J., Zhuo, L., Rong, G.: Estimation of soil moisture using

655   modified antecedent precipitation index with application in landslide predictions. Landslides 16,

656   2381–2393, 2019b.

657 Zhu, Y.J., Shao, M.G.: Variability and pattern of surface moisture on a small-scale hillslope in

658   Liudaogou catchment on the northern Loess Plateau of China, Geoderma, 147, 185-191, 2008.

659 Zhuang, J.Q., Cui, P., Wang, G.H., Chen, X.Q., Iqbal, J., Guo, X.J.: Rainfall thresholds for the

660   occurrence of debris flows in Jiangjia Gully, Yunnan Province, China. Eng. Geol. 195, 335–346,

661   2015.